ChemComm

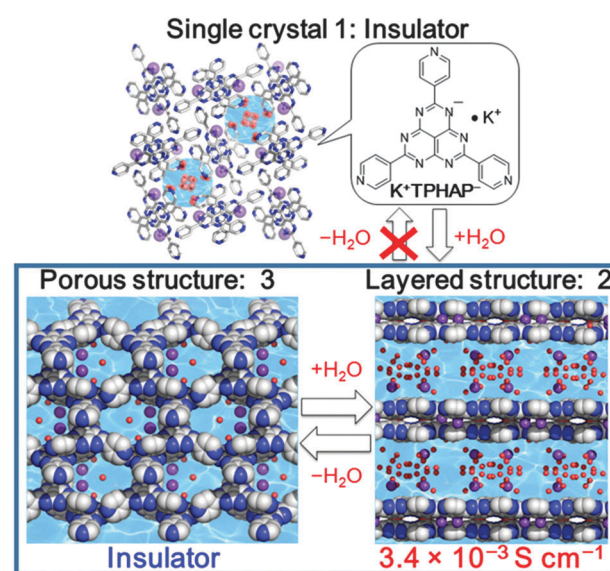# Formation of a nanometer-thick water layer at high humidity on a dynamic crystalline material composed of multi-interactive molecules†

Yumi Yakiyama,‡[a] Gil Ryeong Lee,‡[a] Sung Yeon Kim,[a] Yoshitaka Matsushita,[b] Yasushi Morita,[c] Moon Jeong Park[ad] and Masaki Kawano*[a]

Crystalline powders self-assembled from interactive discrete molecules reversibly transformed from a porous structure to a 2D one with a nanometer-thick H_2O layer by hydration/dehydration. Multi-point weak intermolecular interactions contributed to maintenance of each phase. This structure transformation induced a humidity-dependent ion conductivity change from insulator to 3.4×10^{-3} S cm^{-1}.

Intermolecular interactions participate in emerging functions in functional materials[1] and biological systems.[2] Especially, multi-interactive interactions contribute to stabilizing key meta-stable intermediates in biological processes, because the multiple interactions can deepen the local minimum potential well to trap kinetic states.[3] Therefore, we aimed to implement multi-interactivity into a ligand to achieve kinetically self-assembled networks.[4] We designed a multi-interactive ligand, tri(4-pyridyl)hexaazaphenalene anion (TPHAP⁻), and succeeded in trapping meta-stable coordination networks.[5] In the process, we unexpectedly prepared crystalline self-assembled materials composed of K⁺TPHAP⁻ under highly hydrated conditions. Here we report a 1.2 nm-thick H_2O layer formed of discrete molecules, and the dynamic structure change revealed by X-ray powder diffraction (XRPD) analysis.[6] The ion conductivity σ of the hydrated material changed from insulator to 3.4×10^{-3} S cm^{-1} depending on the amount of intercalated H_2O.

The TPHAP anion has a D_{3h} symmetrical aromatic plane[7] (Scheme 1) that can form π–π stacking interaction, and nine nitrogen atoms that can form hydrogen bonds, coordination bonds, or both.[5] Such multi-interactivity of TPHAP enabled the selective trapping of a kinetic network followed by surface-mediated dynamic structure transformation.[5a] We also prepared various coordination networks composed of Zn²⁺ ions and TPHAP anions from the same crystallization set up by changing only solvents or additives because of the multi-interactivity of TPHAP.[5b,c] The interactive nature of TPHAP was also observed in a 1D-channel structure of a K⁺TPHAP⁻ single crystal **1**. In the crystal, H_2O molecules were encapsulated by OH···N hydrogen bonds with the N atoms on the TPHAP⁻ skeleton (Fig. S1, ESI†). Indeed, the single crystal of K⁺TPHAP⁻ is highly hygroscopic: 1 g of powder of K⁺TPHAP⁻ adsorbs >70 mL of H_2O (at 25 °C, 30% RH) while the potassium salt of the *t*-butyl group substituted hexaazaphenalene (HAP) anion does not

[a] The Division of Advanced Materials Science, Pohang University of Science and Technology (POSTECH), Cheongam-ro 77, Namgu, Pohang 790-784, Korea. E-mail: mkawano@postech.ac.kr; Fax: +82 54 279 8736; Tel: +82 54 279 8740

[b] Research Network and Facility Services Division, National Institute for Materials Science (NIMS), Sengen 1-2-1, Tsukuba, Ibaraki 305-0047, Japan

[c] Department of Applied Chemistry, Faculty of Engineering, Aichi Institute of Technology, Yachigusa 1247, Yakusa, Toyota 470-0392, Japan

[d] Department of Chemistry, Pohang University of Science and Technology (POSTECH), Cheongam-ro 77, Namgu, Pohang 790-784, Korea.

Scheme 1 Schematic model of structure transformation of K⁺TPHAP⁻ depending on the humidity.

show any hygroscopic nature.[7b] K^+TPHAP$^-$ powder retained its crystallinity after hydration.

Therefore, we measured the XRPD pattern of fully-hydrated powder **2** which was prepared by hydration of K^+TPHAP$^-$ single crystals **1** at 95% RH and 25 °C for 1 day (Fig. 1). The XRPD pattern of **2** showed a drastic and irreversible change from initial K^+TPHAP$^-$ single crystalline powder **1** while maintaining a surprisingly high crystallinity. We also identified how the structure changed during drying. We gradually dried fully-hydrated powder **2** by keeping it at 20% RH and 20 °C for 20 s, then quickly measured its XRPD pattern in an airtight cell to avoid further drying during the measurement. This quick drying operation was repeated three times. After the first 20 s, the XRPD pattern was almost intact; the next 20 s of drying induced drastic changes in the XRPD pattern, and a further 20 s of drying (total 1 min) produced a new phase close to the final state, *i.e.*, 1 day dried powder **3** (Fig. S2, ESI†). Notably, the sharp powder pattern of **2** was recovered by rehydration of **3**. This hydration/dehydration process between **2** and **3** was reversible.

To reveal the reversible structure transformation observed during the hydration/dehydration process, we performed XRPD structure analyses of fully-hydrated powder **2**, 1 min dried powder, and 1 day dried powder **3**. The structures were determined by the simulated annealing method in DASH,[8] followed by Rietveld refinement using RIETAN-FP[9] to refine the position of each atom with soft bond-angle restraints for a TPHAP$^-$ group. As a result, we revealed that 1.2 nm H_2O layers form in the fully-hydrated **2** (Scheme 1) and that 1D H_2O channels form in **3** by dehydration. Powder structure analysis of 1 min dried powder revealed a severely disordered structure which was an intermediate state before reaching the state of 1 day dried **3** (Fig. S2, ESI†). It should be noted that although the powder patterns of the 1 min dried powder and **3** look very similar,
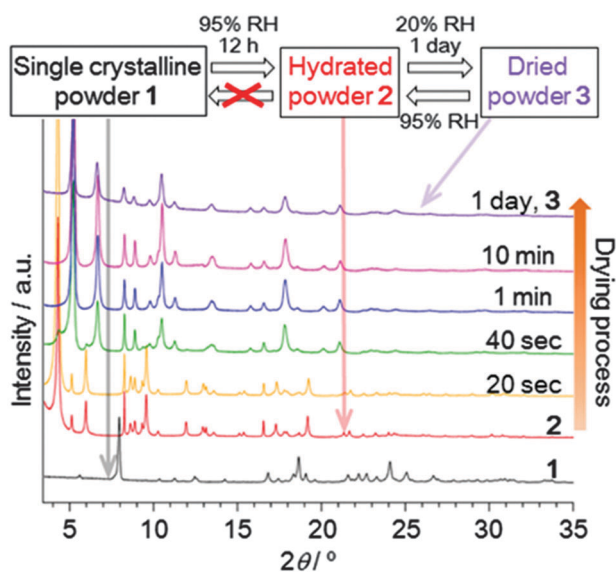

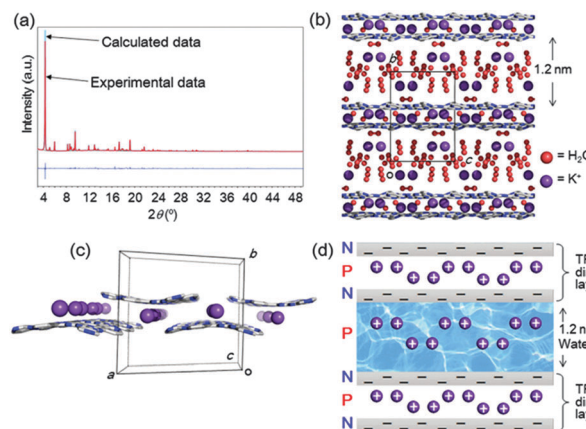Fig. 1 Synchrotron XRPD pattern changes depending on the amount of water in **1**.

Fig. 2 XRPD analysis of fully-hydrated powder **2**. (a) Experimental (red), calculated (pale blue), and difference (blue) diffraction patterns of the best matching model obtained by the final Rietveld refinement of **2**. (b) The best matching model having a 2D layered structure. Synchrotron X-ray radiation λ = 1.4639 Å. Cell parameter: a = 24.131(5) Å, b = 19.458(2) Å, c = 16.672(4) Å, β = 122.52(2)°. (c) 2D-sheet composed of K^+TPHAP$^-$ dimer-like layers. (d) Schematic model of a charged stacking layer structure. P: "positively charged layer"; and N: "negatively charged layer". Color code: C, gray; N, blue; K, purple; O of H_2O, red.

their unit cells are very different (1 min dried powder: a = 20.656(6) Å, b = 15.978(4) Å, c = 16.80(1) Å, β = 100.68(3)°, V = 5449(4) Å^3, $P2/a$; **3**: a = 20.90(1) Å, b = 15.93(1) Å, c = 9.711(5) Å, β = 104.65(3)°, V = 3128(3) Å^3, $P2/a$).

The powder analysis of **2** revealed four equally possible models that have monoclinic $P2/n$ systems that show good agreement between the calculated and experimental XRPD patterns in the final Rietveld refinement (Fig. S3, ESI†). Among them, one (Fig. 2b) showed the best agreement with the experimental data (Fig. 2a and b). Although the precise determination of disordered H_2O and K^+ positions was technically difficult, every refinement result showed flat 2D-sheets composed of K^+TPHAP$^-$ dimer-like layers (Fig. 2c) forming 1.2 nm-thick H_2O layers. These dimer-like layers are stabilized by the intermolecular interactions between the N atoms of the central HAP skeleton and the disordered K^+ ions. These interactions are strong enough to be detected by CSI-MS.[5b] Some pyridine groups of TPHAP$^-$ are close to each other, but the short contact can be explained by severe disorder. The amount of H_2O calculated from XRPD analysis is 31H_2O molecules per K^+TPHAP$^-$ unit, which is close to the maximum value obtained by direct weight measurement (12–28H_2O molecules per K^+TPHAP$^-$ unit, Table S1, ESI†). Notably, other disordered K^+ ions were dispersed in the 1.2 nm water layer. Therefore, stabilization of this H_2O layer is probably due to a large number of H-bonding interactions between H_2O molecules and TPHAP skeletons at the boundary and K^+ ions on the inner part of the H_2O layer. In addition, the whole structure is constructed as alternating stacks of positively-charged large H_2O layers and TPHAP$^-$ dimer-like layers, which are composed of a negatively-charged TPHAP sheet and a positively-charged K^+ layer (Fig. 2d). This electrically neutral arrangement contributes to stabilization of the 2D layered stacking structure.

Pulsed-Field-Gradient ^{1}H-NMR measurement of **2** strongly supported the hypothesized formation of an H_2O layer with a liquid-like state (Fig. S4, ESI†). Solid state ^{1}H-NMR measurement of **1** (as control) and **2** revealed only one peak corresponding to internal H_2O at $\delta = 5.1$ and 4.4 ppm, respectively. The peak corresponding to **1** was small and broad due to a much smaller amount of H_2O in **1** than in **2**. Furthermore, the large number of hydrogen bonds between H_2O molecules and the TPHAP$^-$ skeleton in **1** reduced the mobility of H_2O.[10] In contrast, compared to **1**, H_2O in fully-hydrated powder **2** could move more freely to give a sharper and larger signal. The diffusion coefficient D_{H_2O} of water in **2** was obtained from the plot of spin-echo intensity $I/I_0 = \exp[-D\gamma^2 g^2 \delta^2(\Delta - \delta/3)]$ against the gradient strength g,[11] where I and I_0 are the signal intensities with each g and without g, respectively, and γ is the gyromagnetic ratio. Applied gradient strengths reached 800 G cm^{-1} while gradient δ and gradient delay Δ time values were 0.5 ms and 3.55 ms, respectively. The obtained D_{H_2O} value was 1.0×10^{-9} m^2 s^{-1}, which is close to the self-diffusion coefficient of pure H_2O at rt (*ca.* 2×10^{-9} m^2 s^{-1}).[12] This quite high D_{H_2O} value indicates that the diffusion speed of H_2O molecules in **2** is similar to that in bulk H_2O.

The structural effect of dehydration on the 2D layered structure was also revealed by the XRPD analysis of 1 day dried powder **3** which showed the formation of a porous structure having a monoclinic $P2/a$ system with excellent agreement between the calculated and experimental XRPD patterns in the final Rietveld refinement (Fig. 3). In the crystal structure, the ordered TPHAP$^-$s also maintain dimer-like structures connected by K$^+$ ions and interact with each other by π–π stacking

to form a 2D layer (Fig. 3b and c). The 2D layers stack with the shortest distance (Fig. 3d), followed by formation of 1D channels along the c axis with a size of *ca.* 12 Å × 16 Å (Fig. 3e). In the XRPD analysis, we could model only two H_2O molecules per K$^+$TPHAP$^-$ unit in the channel, although elemental analysis indicated five H_2O molecules per K$^+$TPHAP$^-$ unit. Notably, the 1D channel is surrounded by N atoms on a HAP skeleton as observed in a K$^+$TPHAP$^-$ single crystal **1** in which K$^+$ ions and H_2O molecules are less mobile than in **2**. Therefore, the significant mobility decrease of K$^+$ ions and H_2O was expected as a result of the structural transformation from a 2D-layered structure to a 1D-porous structure. This reduction is also suggested by humidity-dependent IR spectra (Fig. S5, ESI†). As the amount of absorbed H_2O decreased, the peaks at ~1500–1600 cm^{-1} attributable to the C=N and C=C stretching modes of pyridine and the central skeleton of TPHAP$^-$ showed clear red shifts: ~10 cm^{-1} from the fully-hydrated powder **2** to single crystal **1**; 4–5 cm^{-1} from **2** to 1 day dried powder **3**. These peak shifts can be explained by enhancement of Coulombic interaction between K$^+$ and the anionic HAP skeleton and by hydrogen bond formation between TPHAP$^-$ and H_2O.[13] This discussion indicates that this dynamic structure transformation can make a significant contribution to the ion conductivity of K$^+$TPHAP$^-$ because the conductivity value has a strong relationship with charge carrier mobility.[14] Therefore, we finally performed humidity-dependent ion conductivity measurement and tried to interpret the relationship between the structure and the conduction property.

The ion conductivity of K$^+$TPHAP$^-$ single crystalline powder **1** was significantly correlated with the outer humidity. We measured the ion conductivity of a compressed pellet of **1** (ϕ 13 mm, thickness ~0.2 mm) by *ac* impedance spectroscopy under various conditions of humidity and temperature (ESI†). The conductivity drastically changed from insulator at 20% RH to 3.4×10^{-3} S cm^{-1} at 95% RH (25 °C, Fig. 4). Although a large amount of H_2O adsorption in the highly conductive state was observed (Table S1, ESI†), the pellet of **1** remained soft and solid after conductivity measurement (Fig. S6, ESI†). We unambiguously confirmed that the highly-conductive state corresponds to **2** having a 2D layered structure by XRPD measurement of the pellet sample (Fig. S7, ESI†). In contrast, drying of the fully-hydrated pellet even for several seconds reduced its conductivity value significantly. This phenomenon reminded us of the quick structural transformation of **2** to the dried state **3**. We confirmed by XRPD
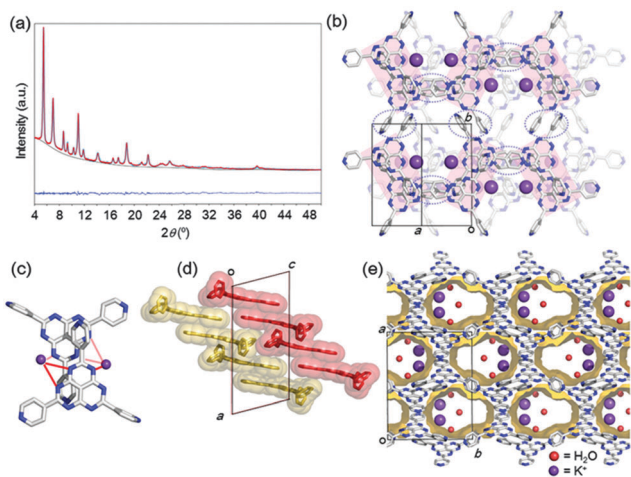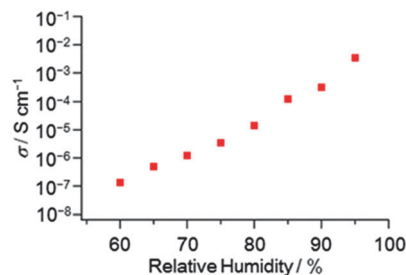
Fig. 3 XRPD analysis of 1 day dried powder **3**. (a) Experimental (red), calculated (pale blue), and difference (blue) diffraction patterns after the Rietveld refinement. X-ray radiation $\lambda = 1.5406$ Å. Cell parameter: $a = 20.90(1)$ Å, $b = 15.93(1)$ Å, $c = 9.711(5)$ Å, $\beta = 100.65(3)$°. (b) 2D layered structure formed by π–π stacking of dimer-like TPHAP$^-$s (pale red rectangles). Pale blue dotted circles: stacking position. (c) Dimer-like structure composed of two K$^+$TPHAP$^-$s. Red lines: ionic bond between the N atom and K$^+$. (d) Stacking structure of 2D layered structures. Red and yellow components represent layers. (e) 1D channel structure in **3**. Color code: C, gray; N, blue; K, purple; O of H_2O, red.

Fig. 4 Humidity dependence of the ionic conductivity σ of **1** at 25 °C.

analysis that the dried pellet corresponds to **3** which possesses a porous structure (Fig. S6, ESI†). Because the system contains no mobile proton (H⁺),[15] the main charge carrier is very likely K⁺. In fact, the K⁺-exchanged proton conducting polymer shows $\sigma = \sim 3.0 \times 10^{-2}$ S cm^{-1} (fully-hydrated at 25 °C) which gives the diffusion coefficient of K⁺ rather than of H⁺.[16] These facts indicate that the main carrier that contributes to ion conductivity is a metal cation. From the above discussion, this drastic conductivity change can be explained based on the changes of the structure and the amount of water in the system. In the hydrated state of **2**, K⁺ can readily diffuse by weak van der Waals interaction with H₂O within the 1.2 nm H₂O layer because the diffusion rate of H₂O is almost the same as that of bulk H₂O. This wide H₂O layer also contributes to the smooth migration of K⁺ by keeping away K⁺ from the surface of the TPHAP⁻ layer. This effective K⁺ migration supported by the fast diffusion of bulk-like H₂O realized the high conductivity under humid conditions. Oppositely, the structure transformation of **2** to porous **3** by drying causes a significant decrease in the mobility of K⁺ ions and H₂O; the large amount of H₂O removal involving this structure transformation increases the contribution of strong H-bonds between N atoms on the TPHAP skeleton and K⁺ or H₂O compared to that in **2**. Therefore, the significant conductivity decrease by dehydration is attributed to the decreased mobility of K⁺ and H₂O due to structural transformation from the 2D-layered structure to the interactive 1D-porous structure.

We revealed formation of a nanometer-thick H₂O layer on a multi-interactive ligand, K⁺TPHAP⁻, by XRPD analysis. We also found reversible shrinkage/expansion of the hydrated powder by dehydration/hydration. This structural transformation corresponded to a drastic change of ion conductivity from insulator to 3.4×10^{-3} S cm^{-1}. Our material may provide better understanding of the correlation between the structure and the physical properties of H₂O- or humidity-triggered functional materials.

Notes and references

1 *Supramolecular Chemistry*, ed. J. W. Steed and J. L. Atwood, Wiley, Chichester, UK, 2nd edn, 2009.
2 (*a*) D. Stock, A. G. W. Leslie and J. E. Walker, *Science*, 1999, **286**, 1700–1705; (*b*) N. Ban, P. Nissen, J. Hansen, P. B. Moore and T. A. Steitz, *Science*, 2000, **289**, 905–920; (*c*) N. H. Joh, A. Min, S. Faham, J. P. Whitelegge, D. Yang, V. L. Woods, Jr. and J. U. Bowie, *Nature*, 2008, **453**, 1266–1270; (*d*) D. M. Rosenbaum, S. G. F. Rasmussen and B. K. Kobilka, *Nature*, 2009, **459**, 356–363.
3 (*a*) M. M. Gromiha and S. Selvaraj, *Prog. Biophys. Mol. Biol.*, 2004, **86**, 235–277; (*b*) M. Chaplin, *Nat. Rev. Mol. Cell Biol.*, 2006, **7**, 861–866.
4 (*a*) M. Kawano, T. Haneda, D. Hashizume, F. Izumi and M. Fujita, *Angew. Chem., Int. Ed.*, 2008, **47**, 1269–1271; (*b*) J. Martí-Rujas, Y. Matsushita, F. Izumi, M. Fujita and M. Kawano, *Chem. Commun.*, 2010, **46**, 6515–6517; (*c*) H. Kitagawa, H. Ohtsu and M. Kawano, *Angew. Chem., Int. Ed.*, 2013, **52**, 12395–12399.
5 (*a*) Y. Yakiyama, A. Ueda, Y. Morita and M. Kawano, *Chem. Commun.*, 2012, **48**, 10651–10653; (*b*) T. Kojima, T. Yamada, Y. Yakiyama, E. Ishikawa, Y. Morita, M. Ebihara and M. Kawano, *CrystEngComm*, 2014, **16**, 6335–6344.
6 (*a*) M. Takata, B. Umeda, E. Nishibori, M. Sakata, Y. Saito, M. Ohno and H. Shinohara, *Nature*, 1995, **377**, 46–49; (*b*) S. Pagola, P. W. Stephens, D. S. Bohle, A. D. Kosar and S. K. Madsen, *Nature*, 2000, **404**, 307–310; (*c*) *IUCr Monographs on Crystallography 13*, ed. W. I. F. David, D. Shankland, L. B. McCusker and C. Baerlocher, Oxford University Press, Oxford, UK, 2002; (*d*) K. D. M. Harris and E. Y. Cheung, *Chem. Soc. Rev.*, 2004, **33**, 526–538; (*e*) J. Martí-Rujas and M. Kawano, *Acc. Chem. Res.*, 2013, **46**, 493–505.
7 (*a*) S. Suzuki, Y. Morita, K. Fukui, K. Sato, D. Shiomi, T. Takui and K. Nakasuji, *Inorg. Chem.*, 2005, **44**, 8197–8199; (*b*) S. Suzuki, K. Fukui, A. Fuyuhiro, K. Sato, T. Takui, K. Nakasuji and Y. Morita, *Org. Lett.*, 2010, **12**, 5036–5039.
8 W. I. F. David, K. Shankland and N. Shankland, *Chem. Commun.*, 1998, 931–932.
9 F. Izumi and K. Momma, *Solid State Phenom.*, 2007, **130**, 15–20.
10 S. Hietala, S. L. Maunu, F. Sundholm, T. Lehtinen and G. Sundholm, *J. Polym. Sci., Part B: Polym. Phys.*, 1999, **37**, 2893–2900.
11 (*a*) J. E. Tanner, *J. Chem. Phys.*, 1970, **52**, 2523–2526; (*b*) T. A. Zawodzinski, Jr., M. Neeman, L. O. Sillerud and S. Gottesfeld, *J. Phys. Chem.*, 1991, **95**, 6040–6044.
12 M. Holz, S. R. Heil and A. Sacco, *Phys. Chem. Chem. Phys.*, 2000, **2**, 4740–4742.
13 M. Vilkman, A. Lankinen, N. Volk, P. Kostamo and O. Ikkala, *Polymer*, 2010, **51**, 4095–4102.
14 *Modern Electrochemistry vol 1: Ionics*, ed. J. O. Bockris and A. K. N. Reddy, Springer, 2nd edn, 1998.
15 Examples of organic molecule-based water-mediated proton conductors which keep rigid structures in humid condition see; (*a*) M. Sadakiyo, T. Yamada and H. Kitagawa, *J. Am. Chem. Soc.*, 2009, **131**, 9906–9907; (*b*) L. Jiménez-García, A. Kaltbeitzel, W. Pisula, J. S. Gutmann, M. Klapper and K. Müllen, *Angew. Chem., Int. Ed.*, 2009, **48**, 9951–9953; (*c*) M. Yoon, K. Suh, H. Kim, Y. Kim, N. Selvapalam and K. Kim, *Angew. Chem., Int. Ed.*, 2011, **50**, 7870–7873; (*d*) J. M. Taylor, K. W. Dawson and G. K. H. Shimizu, *J. Am. Chem. Soc.*, 2013, **135**, 1193–1196.
16 T. Okada, H. Satou, M. Okuno and M. Yuasa, *J. Phys. Chem. B*, 2002, **106**, 1267–1273.